Activation of CH_4 by Gas-Phase Zr^+ and the Thermochemistry of Zr−Ligand Complexes

P. B. Armentrout* and M. R. Sievers†

Department of Chemistry, University of Utah, Salt Lake City, Utah 84112

Received: December 24, 2002; In Final Form: April 2, 2003

The kinetic energy dependence of the reaction of $Zr^+(^4F)$ with methane has been studied using guided ion beam mass spectrometry. At low energies, the only process observed is dehydrogenation, which is slightly endothermic such that it exhibits a strong isotope effect when CD_4 is used as the reactant. At high energies, products resulting from C−H cleavage processes are appreciable. Modeling of the endothermic reaction cross sections yields the 0 K bond dissociation energies (in eV) of $D_0(Zr^+-CH) = 5.96 \pm 0.22$, $D_0(Zr^+-CH_2) = 4.62 \pm 0.07$, and $D_0(Zr^+-CH_3) = 2.30 \pm 0.24$. The experimental thermochemistry is favorably compared with density functional theory calculations (B3LYP), which also establish the electronic structures of these species and provide insight into the reaction mechanism. The results for Zr^+ are compared with those for the first-row transition metal congener Ti^+, and the differences in behavior and mechanism are discussed.

1. Introduction

As part of a long-term project in our laboratory, we are interested in examining periodic trends in the reactions of transition metal ions (M^+) with small hydrocarbons. Extensive work for first-row transition metal elements has revealed the electronic requirements for the activation of C−H and C−C bonds at metal centers[1−4] and provided an examination of the periodic trends in such reactivity unavailable in condensed phase media.[1,2,5] A particular interest in our research is to use guided ion beam methods to obtain metal−hydrogen and metal−carbon bond dissociation energies (BDEs).[6−10] Such thermochemistry is of obvious fundamental interest and also has implications in understanding a variety of catalytic reactions involving transition metal systems.[11] We have recently extended our studies to the reactivity of second-row transition metal cations with small hydrocarbons. This now includes work on Y^+,[12,13] Nb^+,[14] Ru^+,[15] Rh^+,[16,17] Pd^+,[18] and Ag^+,[19] and a review.[20]

In the present study, we extend this work to examine Zr^+ and describe its reactions with methane. This system has been examined at thermal energies by Ranasinghe, McMahon, and Freiser[21] using ion cyclotron resonance (ICR) mass spectrometry. Consequently, only exothermic processes were examined and dehydrogenation was the only process observed. Here, we are able to investigate the reactions of Zr^+ with methane over a wide range of kinetic energies, examining both endothermic and exothermic processes. This permits the extraction of systematic thermodynamic as well as mechanistic information.

There is relatively little thermochemistry available for zirconium species in the literature, as shown in Table 1. We have previously measured BDEs for Zr^+−H, Zr^+−C, and Zr^+−O by determining the endothermicities of the formation of these species from reactions of Zr^+ with H_2 (and D_2)[22] and CO.[23] Bowers and co-workers have measured the binding energies of one to seven H_2 molecules to Zr^+ using equilibrium methods.[24] Photodissociation was used by Ranatunga and Freiser to measure the $Zr^+C_2H_2$ bond energy.[25] In addition, theoretical calculations have been performed for several species relevant to the present work: ZrH^+,[26−29] $ZrCH_2^+$,[29−31] $ZrCH_3^+$,[32] $HZrCH_3^+$, and $Zr^+(CH_4)$.[33] In the present work, we measure several of these BDEs by determining the endothermic reaction thresholds for reactions of Zr^+ with methane. We use a direct current (dc) discharge/flow tube ion source to produce Zr^+ ions that are believed to be in the ^4F electronic ground-state term.[22] Thus, the threshold measurements have few complexities associated with the presence of ions in electronic excited states.

One of the challenging problems in the study of alkane activation by transition metal ions is to determine reaction mechanisms. In contrast to work on first-row transition metal cations (mostly Fe^+, Co^+, and Ni^+), few detailed experimental and theoretical studies have been carried out to elucidate the mechanisms of second-row transition metal cations.[16,17,33,34] Nevertheless, it is clear that the mechanisms for alkane activation do vary with the identity of the metal ions, both from early to late and from first-row to second-row transition metal cations, as we have recently reviewed.[20] Here, we examine the mechanisms for reactions of Zr^+ with methane by a detailed theoretical calculation of the potential energy surfaces involved, including full characterization of all intermediates and transition states on both doublet and quartet spin surfaces. These results are then compared to the mechanisms previously proposed for the analogous reaction of the first-row congener, Ti^+.[35]

TABLE 1: Zr^+−L Bond Energies (eV) at 0 K

	this work		previous work	
species	experiment	theory	experiment	theory
Zr^+−H	2.23 (0.10)	2.55	2.26 (0.08)[a]	2.37,[b] 2.46,[c] 2.46,[d] 2.56[e]
Zr^+−C	4.88 (0.15)	4.60	4.72 (0.11)[f]	
Zr^+−CH	5.96(0.22)	5.50		
Zr^+−CH_2	4.62 (0.07)	4.37		4.38 (0.13),[g] 4.40[h]
Zr^+−CH_3	2.30 (0.24)	2.80		2.48 (0.13)[i]
Zr^+−H_2			0.63 (0.01)[j]	
Zr^+−C_2H_2			2.56 (0.13)[k]	2.95[l]

[a] Reference 22. [b] Reference 26. [c] Reference 27. [d] Reference 28. [e] Reference 29. [f] Reference 23. [g] Reference 30. [h] Reference 31. [i] Reference 32. [j] Reference 24. [k] Reference 25. [l] Sodupe, M.; Bauschlicher, C. W. *J. Phys. Chem.* **1991**, *95*, 8640.

† Present address: IBM, 2070 Route 52 M/S EM1, Hopewell Junction, NY 12533.

10.1021/jp027820d CCC: $25.00
Published on Web 05/13/2003

2. Experimental and Theoretical Section

2.1. General. These studies are performed using a guided ion beam tandem mass spectrometer. The instrument and experimental methods have been described previously.[36,37] Ions, formed as described below, are extracted from the source, accelerated, and focused into a magnetic sector momentum analyzer for mass analysis. For these experiments, the ^{90}Zr isotope (51.5% natural abundance) is used. The ions are decelerated to a desired kinetic energy and focused into an octopole ion guide that radially traps the ions.[38] While in the octopole, the ions pass through a gas cell that contains the neutral reactant at pressures where multiple collisions are improbable (<0.30 mTorr). Single collision conditions were verified by examining the pressure dependence of the cross sections measured here. The product ions and the reactant ion beam drift out of the gas cell, are focused into a quadrupole mass filter, and then are detected by a secondary electron scintillation detector. Ion intensities are converted to absolute cross sections as described previously.[36] Uncertainties in the absolute cross sections are estimated at ±20%.

To determine the absolute zero and distribution of the ion kinetic energy, the octopole is used as a retarding energy analyzer.[36] The uncertainty in the absolute energy scale is ±0.05 eV (lab). The full width at half-maximum (fwhm) of the ion energy distribution is 0.2−0.4 eV (lab). Lab energies are converted into center-of-mass energies using $E(\mathrm{CM}) = E(\mathrm{lab})\text{-}m/(m + M)$, where M and m are the masses of the ion and neutral reactants, respectively. At the lowest energies, the ion energies are corrected for truncation of the ion beam as described previously.[36] All energies referred to below are in the center-of-mass frame.

2.2. Ion Source. The ion source used here is a dc discharge/flow tube (DC/FT) source described in previous work.[37] The DC/FT source utilizes a zirconium cathode held at 1.5−3 kV over which a flow of approximately 90% He and 10% Ar passes at a typical pressure of ~0.5 Torr. Ar^+ ions created in a direct current discharge are accelerated toward the zirconium cathode, sputtering off atomic metal ions. The ions then undergo $\sim 10^5$ collisions with He and $\sim 10^4$ collisions with Ar in the meter-long flow tube before entering the guided ion beam apparatus. Results obtained previously[22] indicate that the ions produced in the DC/FT source are exclusively in their a^4F ground state. This study determined that the electronic temperature is likely to be 300 ± 100 K, such that the average electronic energy of Zr^+ is 0.013 ± 0.004 eV.

2.3. Data Analysis. Previous theoretical[39] and experimental work[40] has shown that endothermic cross sections can be modeled using eq 1:

$$\sigma(E) = \sigma_0 \sum g_i (E + E_{\mathrm{el}} + E_i - E_0)^n / E \qquad (1)$$

where σ_0 is an energy-independent scaling parameter, E is the relative translational energy of the reactants, E_{el} is the average electronic energy of the Zr^+ reactant (noted above), E_0 is the reaction threshold at 0 K, and n is a parameter that controls the shape of the cross section. The summation is over each rovibrational state of the neutral reactant having relative populations g_i and energies E_i. The vibrational frequencies of methane used in this work are taken from the literature.[41]

Before comparison with the data, the model is convoluted over the neutral and ion kinetic energy distributions using previously developed methods.[36] The parameters E_0, σ_0, and n are then optimized using a nonlinear least-squares analysis in order to best reproduce the data. Reported values of E_0, σ_0, and n are mean values for each parameter from the best fits to several independent sets of data, and uncertainties are one standard deviation from the mean. The listed uncertainties in the E_0 values also include the uncertainty in the absolute energy scale and the uncertainty in the electronic energy of Zr^+.

2.4. Theoretical Calculations. All quantum chemistry calculations here are computed with the B3LYP hybrid density functional method[42−44] and performed with the Gaussian 98 suite of programs.[45] In all cases, the thermochemistry reported here is corrected for zero point energy (ZPE) effects (with frequencies scaled by 0.9804).[46] Because several of the transition states of interest here involve bridging hydrogens, the rather large 6-311++G(3df,3p) basis set is used for carbon and hydrogen. This basis set gives good results for the thermochemistry of methane and dihydrogen, with deviations from experiment of less than 0.08 eV for the bond energies (theory vs experiment) of $H-CH_3$ (4.410 vs 4.480 eV), H_2-CH_2 (4.670 vs 4.713 eV), H−CH (4.334 vs 4.360 eV), C−H (3.534 vs 3.465 eV), and H−H (4.508 vs 4.478 eV). The basis on zirconium was the Hay−Wadt ($n + 1$) ECP VDZ (HW),[47] equivalent to the Los Alamos ECP (LANL2DZ) basis set, in which 28 core electrons are described by a relativistic effective core potential (ECP).[48]

For many of the species calculated here, calculations of excited states were obtained by explicitly moving electrons into other orbitals to create states of alternate configuration and/or symmetry. Optimizations of the geometry were then carried out in the usual way.

The splitting between the $^4F(5s^14d^2)$ ground state and $^2D(5s^14d^2)$ excited state is calculated to be 0.410 eV. This value should be compared with the experimentally determined 0.452 eV excitation between the averages of properly weighted spin−orbit components of the ^4F (0.094 eV above the $^4F_{3/2}$ ground level) and ^2D (0.546 eV above the $^4F_{3/2}$ ground level) terms.[49] Because our calculations do not explicitly include spin−orbit interactions, all calculations involving an asymptote including Zr^+ are referenced to the average energy of the spin−orbit components of the ^4F term at 0.094 eV. To properly compare to experimental values, which refer to the energy of the $^4F_{3/2}$ ground state at 0.0 eV, the calculated values must be corrected for this different asymptotic energy.

3. Experimental Results

Reaction of Zr^+ with methane yields the products indicated in reactions 2−6.

$$Zr^+ + CH_4 \rightarrow ZrH^+ + CH_3 \qquad (2)$$

$$\rightarrow ZrC^+ + 2H_2 \qquad (3)$$

$$\rightarrow ZrCH^+ + H_2 + H \qquad (4)$$

$$\rightarrow ZrCH_2^+ + H_2 \qquad (5)$$

$$\rightarrow ZrCH_3^+ + H \qquad (6)$$

These results are shown in Figure 1. In some cases, these cross sections have been corrected for mass overlap between product ions having adjacent masses, but in all cases, such corrections are unambiguous. Very similar results were also obtained for analogous reactions with CD_4, where mass overlap problems are greatly reduced. The lowest energy pathway is dehydrogenation of methane to form $ZrCH_2^+$, reaction 5. The cross section rises from a finite magnitude at zero energy of about $(1.5 \pm 0.3) \times 10^{-16}$ cm^2. This agrees very well with the ICR study of Ranasinghe et al.[21] They reported that reaction 5 has

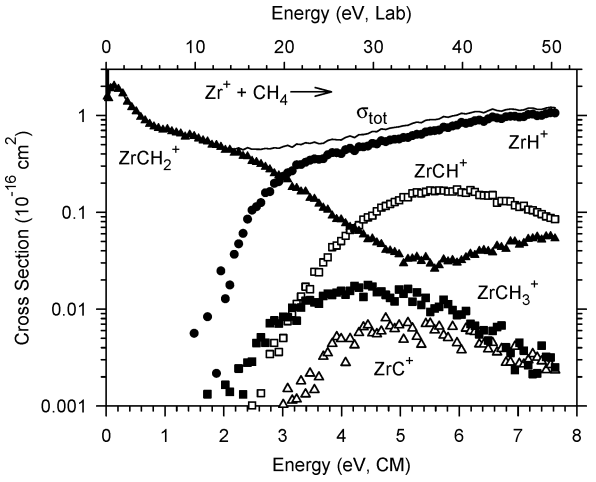

Figure 1. Cross sections for reactions of Zr^+ with CH_4 as a function of kinetic energy in the center-of-mass frame (lower axis) and laboratory frame (upper axis).

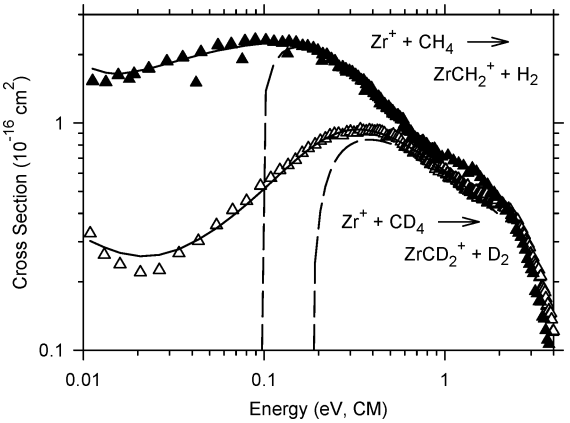

Figure 2. Cross sections for the dehydrogenation reactions of Zr^+ with CH_4 and CD_4 as a function of kinetic energy in the center-of-mass frame (lower axis) and laboratory frame (upper axis). Solid lines show the best fit to the data using the model of eq 1 convoluted over the neutral and ion kinetic and internal energy distributions. Dashed lines show the model cross sections in the absence of experimental kinetic energy broadening for reactions with an internal energy of 0 K.

an efficiency of 0.007 ± 0.004, which corresponds to a cross section at thermal energies (~0.04 eV) of $(1.9 \pm 1.1) \times 10^{-16}$ cm^2. The dehydrogenation reaction is the only process that exhibits a noticeable change upon deuteration. As shown in Figure 2, the analogue of reaction 5 is much less efficient for CD_4 at thermal energies than for CH_4, although the cross sections match one another at higher energies (above about 0.7 eV).

Although the $ZrCH_2^+$ cross section is nonzero at thermal energies, it does increase with increasing energy, rapidly reaching a maximum of $(2.3 \pm 0.5) \times 10^{-16}$ cm^2 at 0.1 eV (the $ZrCD_2^+$ cross section maximizes at $(0.9 \pm 0.2) \times 10^{-16}$ cm^2 and 0.35 eV). Above this energy, the cross section declines approximately as $E^{-0.23\pm0.03}$. Near 2 eV, the $ZrCH_2^+$ (and $ZrCD_2^+$) cross section declines more rapidly, which could be a result of decomposition or competition with another product. $ZrCH_2^+$ can decompose by losing CH_2 to form Zr^+ starting at 4.71 eV = $D_0(H_2{-}CH_2)$, by dehydrogenating to form ZrC^+, or by losing an H atom to form $ZrCH^+$. Clearly the former channel begins too high in energy to account for the decline and the ZrC^+ channel starts too late and is too small to account for all of the decline (Figure 1). Although the $ZrCH^+$ channel has sufficient intensity, it also starts too high in energy (which can be seen by examining the sum of the $ZrCH_2^+$ and $ZrCH^+$ cross sections). Instead, we find that the increase in the ZrH^+ cross section more than compensates for the decline observed in the $ZrCH_2^+$ cross section, indicating that this decline is primarily a result of competition with ZrH^+. This demonstrates that these two products share a common intermediate.

The ZrH^+ cross section rises from an apparent threshold near 2 eV and continues rising at all energies examined. The other primary product formed in this system is $ZrCH_3^+$, formed in reaction 6 and having a similar apparent threshold near 2 eV. The cross section for this product is small, apparently the result of competition with the nearly isoenergetic reaction 2 and rapid dehydrogenation to form $ZrCH^+$. An alternate decomposition pathway for $ZrCH_3^+$ is H atom loss to form $ZrCH_2^+$, which is evident as the rise in the $ZrCH_2^+$ cross section beginning about 5.5 eV. The $ZrCH^+$ and ZrC^+ cross sections begin to rise near 2.5 and 3 eV, respectively. As noted above, the $ZrCH^+$ species comes from dehydrogenation of the primary $ZrCH_3^+$ product. The ZrC^+ product must result from dehydrogenation of the primary $ZrCH_2^+$ product.

4. Thermochemical and Theoretical Results

The energy dependences of the various cross sections are interpreted using eq 1. The optimum values of the parameters of eq 1 are listed for the CH_4 and CD_4 systems in Table 2. The thresholds can then be related to thermodynamic information assuming that this represents the energy of the product asymptote, an assumption that is usually correct for ion−molecule reactions because of the long-range attractive forces. Thus, eq 7 is used to derive the BDEs provided below where R−L is the reactant hydrocarbon.

$$D_0(Zr^+{-}L) = D_0(R{-}L) - E_0 \qquad (7)$$

Because our threshold analyses carefully include all sources of reactant energy, the thermochemistry obtained is for 0 K. Values for $D_0(R{-}L)$ for both CH_4 and CD_4 needed in the following are collected and listed elsewhere.[50] The following sections describe the experimental thermochemistry derived in this fashion for each of the ionic products along with our theoretical characterization of these species. Table 3 summarizes the calculated energies and zero point energies for the various species discussed below along with those needed to determine bond energies.

4.1. ZrH^+. A reliable value for $D_0(Zr^+{-}H)$, Table 1, has previously been determined from the reactions of Zr^+ with H_2 and D_2.[22] Using this BDE, the predicted threshold for the ZrH^+ product in the methane reaction is 2.22 ± 0.08 eV and that for ZrD^+ from CD_4 is 2.29 ± 0.08 eV, using a ZPE difference for ZrH^+ vs ZrD^+ of 0.030 eV.[22] The thresholds measured for this process, Table 2, are nicely consistent with these predictions.

Our theoretical calculations find that the ground state of ZrH^+ is $^3\Phi$, having a valence electron configuration of $\sigma_b^2\delta^1\pi^1$, where σ_b is the bonding orbital and the other orbitals are largely metal-based 4d orbitals. A low-lying $^3\Delta$ state ($\sigma_b^2\delta^1\sigma^1$) lies only 0.04 eV higher in energy. A $^1\Sigma^+$ ($\sigma_b^2\sigma^2/\sigma_b^2\delta^2$) state was also found and calculated to lie 0.88 eV higher in energy than the ground state. These states are found to have bond lengths (r_e) of 1.812, 1.799, and 1.822 Å, respectively. In agreement with these results, Schilling et al.[26] find a $^3\Phi$ ground state with a bond length of $r_e = 1.857$ Å, and several excited states: $^3\Delta$ ($r_e = 1.843$ Å) at 0.065 eV, $^3\Sigma^-$ ($\sigma_b^2\delta^2/\sigma_b^2\pi^2$) ($r_e = 1.866$ Å) at 0.100 eV, and $^3\Pi$ ($\sigma_b^2\delta^1\pi^1/\sigma_b^2\sigma^1\pi^1$) ($r_e = 1.856$ Å) at 0.165 eV. Work by Pettersson et al.[27] finds a ground state of $^3\Delta$ ($r_e = 1.830$ Å) and the $^3\Phi$ ($r_e = 1.845$ Å) state lying 0.05 eV higher in energy.

TABLE 2: Optimized Parameters of Eq 1 for $Zr^+ + CH_4$ System

reactants	products	σ_0	n	E_0, eV	$D_0(Zr^+-L)$, eV
$Zr^+ + CH_4$	$ZrH^+ + CH_3$	0.69 (0.27)	1.3 (0.2)	2.26 (0.14)	2.22 (0.14)
	$ZrC^+ + 2H_2$	0.016 (0.003)	1.0	3.11 (0.11)	4.95 (0.11)
	$ZrCH^+ + H_2 + H$	0.19 (0.08)	2.1 (0.3)	3.09 (0.13)	5.98 (0.13)
	$ZrCH_2^+ + H_2$	0.74 (0.02)	0.3 (0.1)	0.11 (0.07)	4.60 (0.07)
	$ZrCH_3^+ + H$	0.039 (0.012)	1.3 (0.3)	2.16 (0.16)	2.32 (0.16)
$Zr^+ + CD_4$	$ZrD^+ + CD_3$	0.72 (0.32)	1.4 (0.1)	2.30 (0.15)	2.27 (0.15)
	$ZrC^+ + 2D_2$	0.013 (0.003)	1.0	3.4 (0.2)	4.8 (0.2)
	$ZrCD^+ + D_2 + D$	0.43 (0.16)	1.7 (0.4)	3.30 (0.20)	5.95 (0.20)
	$ZrCD_2^+ + D_2$	0.66 (0.13)	0.4 (0.1)	0.19 (0.03)	4.63 (0.03)
	$ZrCD_3^+ + D$	0.048 (0.019)	1.3 (0.2)	2.30 (0.18)	2.27 (0.18)

TABLE 3: B3LYP/HW/6-311++G(3df,3p) Calculated Energies of Reactants and Products[a]

species	state	E (hartree)	ZPE (hartree)	$E + 0.9804$ ZPE	D_0 (eV)[a]
Zr^+	^4F	−46.182 508			
	^2D	−46.167 448			
H	^2S	−0.502 257			
H_2	$^1\Sigma_g^+$	−1.180 030	0.010 066	−1.170 161	4.507
C	^3P	−37.857 471			
CH	$^2\Pi$	−38.495 898	0.006 440	−38.489 584	3.534
CH_2	$^3B_1$	−39.167 949	0.017 161	−39.151 124	4.334
CH_3	$^2A_2''$	−39.857 664	0.029 673	−39.828 573	4.767
CH_4	$^1A_1$	−40.536 527	0.044 503	−40.492 896	4.410
ZrH^+	$^3\Phi$	−46.786 007	0.004 028	−46.782 058	2.553
	$^3\Delta$	−46.784 662	0.004 161	−46.780 583	2.513
	$^1\Sigma^+$	−46.753 567	0.004 074	−46.749 573	1.670
ZrC^+	$^2\Sigma^+$	−84.214 407	0.002 164	−84.212 285	4.595
	$^4\Sigma^-$	−84.181 664	0.001 833	−84.179 867	3.713
	$^4\Delta$	−84.179 557	0.001 833	−84.177 760	3.655
	$^2\Sigma^+$	−84.167 070	0.001 825	−84.165 281	3.316
	$^2\Delta$	−84.142 173	0.001 968	−84.140 244	2.634
	$^4\Phi$	−84.126 282	0.001 411	−84.124 899	2.217
$ZrCH^+$	$^1\Sigma^+$	−84.889 943	0.012 484	−84.877 704	5.501
	$^3\Phi$	−84.859 221	0.011 854	−84.847 599	4.682
	$^3\Delta$	−84.816 248	0.011 287	−84.805 182	3.527
$ZrCH_2^+$	$^2A'$	−85.518 154	0.020 993	−85.497 572	4.367
	$^2A''$	−85.513 651	0.020 912	−85.493 149	4.247
	$^4B_2$	−85.488 214	0.020 752	−85.467 869	3.559
	$^4A_2$	−85.420 108	0.018 586	−85.401 886	1.763
	$^4B_1$	−85.328 918	0.017 395	−85.311 864	−0.686
$ZrCH_3^+$	^3E	−86.148 855	0.031 922	−86.117 559	2.803

[a] Bond energies for H−H, CH_{n-1}−H, or Zr^+−L. The latter have been corrected for the average spin−orbit level of 0.094 eV.

Likewise, Das and Balasubramanian[28] performed complete active space (CASSCF) calculations followed by second-order configuration interaction (SOCI) calculations with a relativistic ECP on Zr to obtain a $^3\Delta$ (r_e = 1.825 Å) ground state, $^3\Phi$ (r_e = 1.841 Å) at 0.077 eV, $^3\Sigma^-$ (r_e = 1.842 Å) at 0.171 eV, $^3\Pi$ (r_e = 1.843 Å) at 0.273 eV, and the $^1\Sigma^+$ state (r_e = 1.837 Å) at 0.349 eV, as well as two more triplet states and three singlet states lying higher in energy (from 0.387 to 1.096 eV). Overall, identification of the true ground state ($^3\Phi$ or $^3\Delta$) does not seem possible from any of these calculations.

The ground-state bond energies calculated in each of these studies are included in Table 1 along with the PCI-80 value from Siegbahn et al.[29] and the present theoretical result. The present result, which includes ZPE corrections and an adjustment for the spin−orbit level of Zr^+, agrees well with these previous investigations, but in all cases, the theoretical values are slightly higher than the experimental value. Possible reasons for such a discrepancy have been discussed,[22] although no plausible experimental artifact could be identified.

4.2. ZrC^+. A value for $D_0(Zr^+-C)$, Table 1, has previously been determined from the reactions of Zr^+ with CO.[23] Using this BDE, the predicted threshold for the ZrC^+ product in the methane reaction is 3.34 ± 0.11 eV and is 3.48 ± 0.11 eV in the CD_4 system. The magnitudes of this product cross section are sufficiently small that analysis in which all parameters of eq 1 are allowed to optimize is not possible; however, thresholds consistent with the predictions are obtained when the value of n is held to unity, Table 2.

The $C(^3P,s^2p^2)$ atom should be able to form two covalent bonds with Zr^+ and possibly augment these bonds by sharing the pair of s electrons on carbon. Our theoretical calculations verify this and find that the ground state of ZrC^+ is $^2\Sigma^+$, having a valence electron configuration of $\pi_b^4\sigma_b^1$, where all orbitals have considerable bonding character. (There is also a doubly occupied σ orbital that is largely composed of the 2s electrons on C, which is not listed explicitly for simplicity.) The σ orbital is largely $4d_{z^2}(Zr) + 2p_z(C)$, whereas the π_b orbitals are the obvious combinations of $4d_{xz,yz}$ and $2p_{x,y}$ orbitals. Another $^2\Sigma^+$ state ($\pi_b^4\sigma^1$), which lies 1.29 eV higher in energy, has a singly occupied σ orbital that is largely metal 5s. A $^2\Delta$ state ($\pi_b^4\delta^1$) lies 1.97 eV higher than the ground state, and several quartet spin excited states were also identified: a $^4\Sigma^-$ state ($\sigma_b^2\pi_b^2\sigma^1$) at 0.89 eV, a $^4\Delta$ state ($\sigma_b^2\pi_b^2\delta^1$) at 0.95 eV, and a $^4\Phi$ state ($\sigma_b^2\pi_b^1\delta^1\sigma^1$) at 2.40 eV. The doublet states are found to have bond lengths (r_e) of 1.778, 1.921, and 1.833 Å, respectively, whereas the quartet states have lengths of 1.921, 1.921, and 2.129 Å, respectively. The bond energy calculated for the $^2\Sigma^+$ ground state is 4.60 eV, including ZPE corrections and adjustment for the spin−orbit level of Zr^+. This value agrees well with our experimental value, Table 1.

4.3. $ZrCH^+$. The thresholds obtained from the $ZrCH^+$ cross sections result in $D_0(Zr^+-CH)$ of 5.98 ± 0.13 and 5.92 ± 0.20 eV for the CH_4 and CD_4 systems, respectively, after making a ZPE correction of 0.024 eV for $ZrCD^+$ (calculated from theoretical vibrational frequencies). We take the weighted average of these two values to obtain 5.96 ± 0.22 eV (where the uncertainty is two standard deviations of the mean) as our best value for $D_0(Zr^+-CH)$.

The $CH(^4\Sigma^-)$ fragment should be able to form a triple bond with Zr^+, although this requires excitation from the $^2\Pi$ ground state. Our theoretical calculations verify that the $^1\Sigma^+$ ground state of $ZrCH^+$ has a covalent triple bond, with a valence electron configuration of $\sigma_b^2\pi_b^4$, where all orbitals have considerable bonding character. (Again the doubly occupied σ orbital that is largely composed of the 2s electrons on C has been omitted for simplicity.) This molecule is linear with $r_e(ZrC) = 1.807$ Å and $r_e(CH) = 1.089$ Å. Two triplet excited states were also identified: a $^3\Phi$ ($\sigma_b^2\pi_b^3\delta^1$) state lying 0.84 eV above the ground state, $r_e(ZrC) = 1.928$ Å and $r_e(CH) = 1.089$ Å; and a $^3\Delta$ ($\sigma_b^2\pi_b^2\delta^1\sigma^1$) state lying 2.01 eV above the ground state, $r_e(ZrC) = 2.097$ Å and $r_e(CH) = 1.089$ Å. The bond energy calculated for the $^1\Sigma^+$ ground state is 5.50 eV, including ZPE corrections and adjustment for the spin−orbit level of Zr^+. This value is somewhat below our experimental value, but both are substantially stronger than $D_0(Zr^+-C)$, consistent with the relative bond order expected.

4.4. $ZrCH_2^+$. The dominant reaction in the methane systems is dehydrogenation, reaction 5. Despite the fact that this process is observed at room temperature,[21] the kinetic energy dependence of this cross section makes it obvious that this is an endothermic process in the CH_4 system. This conclusion is made unambiguous in the CD_4 system because dehydrogenation requires an additional 0.11 eV ($D_0(CH_2-H_2) = 4.713$ eV vs $D_0(CD_2-D_2) = 4.822$ eV and the difference between $D_0(Zr^+-CH_2)$ and $D_0(Zr^+-CD_2)$ is only 0.003 eV according to theoretical calculations). Analysis of these cross sections is complicated because of the very low thresholds involved, which means uncertainties in the absolute energy scale, and the exact form of the various energy convolutions needs to be carefully considered. Further, analyses in which eq 1 is multiplied by a factor of $E^{-0.5}$ to account for the spin change in this reaction (see below) yield n parameters that seem more physically realistic, although the threshold energies are not sensitive to this alteration. Our best fits to the data are shown in Figure 2 and have required that uncertainties in the energy scale be considered. Overall, the thresholds determined are not sensitive to the various treatments and the differences in the thresholds for the CH_4 and CD_4 systems are consistent with the expected zero point energy shift. Our measurements of the threshold for reaction 5 and its perdeuterated analogue result in $D_0(Zr^+-CH_2) = 4.60 \pm 0.04$ and 4.63 ± 0.04 eV, respectively, after making a ZPE correction of 0.003 eV for $ZrCD_2^+$. These values are quite consistent, and we adopt the weighted average of the two as our best value, yielding 4.62 ± 0.07 eV (two standard deviations of the mean).

The $CH_2(^3B_1)$ fragment should be able to form two covalent bonds with Zr^+, which should yield a doublet ground state. Indeed, Bauschlicher et al.[30] reported a $^2A_1$ ground state having the anticipated C_{2v} geometry, with a $^2A_2$ state lying only 0.10 eV higher in energy. Our theoretical calculations find a $^2A'$ ground state for $ZrCH_2^+$ with the geometry distorted from C_{2v}, as shown in Figure 3. A similar distorted ground-state structure has recently been identified theoretically for WCH_2^+ as well.[51] We also find a $^2A''$ state lying 0.12 eV higher in energy. When the calculations are constrained to C_{2v} symmetry, we find the corresponding $^2A_1$ and $^2A_2$ states (both of which have an imaginary frequency), which have geometries similar to those calculated by Bauschlicher et al. These lie only 0.07 and 0.05 eV above the $^2A'$ and $2A''$ states, respectively, such that the $^2A_2$ state lies above the $^2A_1$ by 0.10 eV, in agreement with the previous calculations. We also identified a $^4B_2$ excited state lying 0.81 eV above the $^2A'$ ground state and having the geometry shown in Figure 3. Higher lying quartet states include $^4A_2$ and $^4B_1$ states at 2.60 and 5.05 eV above the $^2A'$ ground state. The bond energy calculated for the $^2A'$ ground state is 4.37 eV, including ZPE corrections and adjustment for the spin−orbit level of Zr^+. This value agrees nicely with that from Bauschlicher et al.[30] and the PCI-80 result of Blomberg and Siegbahn,[31] Table 1.

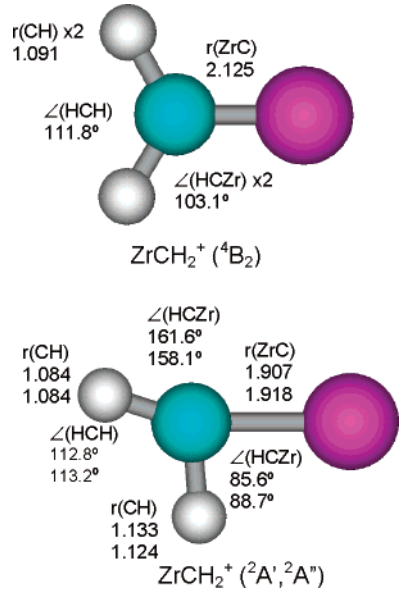

Figure 3. Ground-state geometries of $ZrCH_2^+$ for both the lowest energy quartet state ($^4B_2$) and the two low energy doublet states ($^2A'$, upper values; $^2A''$, lower values). Bond lengths are in angstroms and angles are in degrees. All structures were optimized at the B3LYP/HW/6-311++G(3df,3p) level of theory.

The experimental value is slightly higher than the theoretical values. Agreement between our measured values and those calculated by Bauschlicher for many other transition metal methylidene cations has been good,[9,12−18] although the disagreement is worse for the $NbCH_2^+$ BDE.[14] The data in the methane system leave no doubt that the Zr^+-CH_2 BDE cannot be as low as 4.4 eV. The discrepancy cannot be a result of a barrier to these reactions in excess of the endothermicity as this would raise our measured BDE. The only possible means of lowering the experimentally determined BDE is if there are unaccounted sources of reactant energy, such as higher energy spin−orbit states that are much more reactive than lower energy spin−orbit states. However, there are no experimental indications of such states, and the presence of such states would also lower our experimental bond energies for ZrH^+ and $ZrCH_3^+$, which are already lower than the theoretical values.

4.5. $ZrCH_3^+$. The thresholds obtained for the $ZrCH_3^+$ cross sections in the CH_4 and CD_4 systems result in $D_0(Zr^+-CH_3)$ of 2.32 ± 0.16 and 2.27 ± 0.18 eV, respectively, after making a ZPE correction of 0.003 eV for $ZrCD_3^+$ (calculated from theoretical vibrational frequencies). The weighted average of these values is 2.30 ± 0.24 eV, which compares well with the theoretical value of 2.48 eV given by Bauschlicher et al.[32] This identifies this species as the zirconium methyl cation.

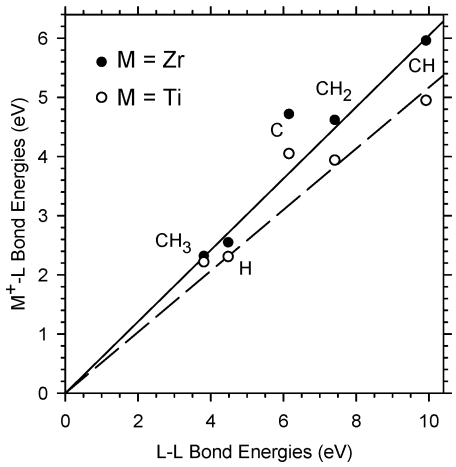

Figure 4. Correlation of Zr^+-L and Ti^+-L bond energies with those for the organic analogues, L−L. Zr^+-L values are from Table 1, and Ti^+-L values are from ref 35. Lines are linear regression fits to the data, excluding MC^+, constrained to pass through the origin.

Bauschlicher et al.[32] reported a ^3E ground state having the anticipated C_{3v} geometry with $r_e(ZrC) = 2.168$ Å and $\angle(ZrCH) = 109.5°$. A $^3A_2$ state lying only 0.23 eV higher in energy was also found. Our theoretical calculations also find a ^3E ground state, with $r_e(ZrC) = 2.133$ Å, $r_e(CH) = 1.096$ Å, $\angle(ZrCH) = 109.2°$, and $\angle(HCH) = 109.8°$. The bond energy calculated for the ^3E ground state is 2.80 eV, including ZPE corrections and adjustment for the spin−orbit level of Zr^+. The inaccuracy of this calculation is not unique. Difficulties with the ability of the B3LYP hybrid functional to determine accurate bond energies for transition metal methyl cations has been commented on previously.[52] For instance, the first row congener of the $ZrCH_3^+$ species, $TiCH_3^+$, had a bond energy calculated using B3LYP that is 0.8 eV higher than experiment and 0.5−1.0 eV higher than other theoretical methods (BHLYP, QCISD, QCISD(T), and MCPF) as well.

4.6. Bond-Energy Bond-Order Correlation for Zr^+-CH_x Bonds. One interesting way of investigating the bond order of simple metal ligand species is to compare with organic analogues, i.e., $D_0(Zr^+-L)$ vs $D_0(L-L)$.[53] Such a plot is shown in Figure 4, with a linear regression fit to the data excluding ZrC^+. It can be seen that the correlation is quite good, which indicates that Zr^+-H and Zr^+-CH_3 are single bonds, $Zr^+=CH_2$ is a double bond, and $Zr^+\equiv CH$ is a triple bond. The point that lies furthest from the line is for Zr^+-C, correlated with the BDE of C_2. In this case, the ZrC^+ BDE lies above the line because the covalent double bond in this molecule (essentially two π bonds, as for C_2) can be augmented by back-donation of an occupied 4dσ orbital on Zr^+ into the empty 2pσ orbital on C, something that C_2 cannot do.

5. Potential Energy Surface of $[ZrCH_4]^+$

In constructing a potential energy surface (PES) for the interaction of $Zr^+(^4F) + CH_4(^1A_1)$, we first consider the spin states of all the various product channels. Calculations here and in the literature (see discussion above) indicate that the dehydrogenation process forming $ZrCH_2^+(^2A') + H_2(^1\Sigma_g^+)$ is spin-forbidden, although formation of the excited state, $ZrCH_2^+(^4B_2) + H_2(^1\Sigma_g^+)$, would be spin-allowed, as would formation of ground-state products starting with $Zr^+(^2D)$. The subsequent dehydrogenation, $ZrCH_2^+(^2A') \rightarrow ZrC^+(^2\Sigma^+) + H_2(^1\Sigma_g^+)$, is spin-allowed, but again spin-forbidden from ground-state reactants. Formations of $ZrH^+(^3\Phi/^3\Delta) + CH_3(^2A_2'')$ and $ZrCH_3^+(^3E) + H(^2S)$ are spin-allowed starting from either quartet or doublet reactant ions. The subsequent dehydrogenation process of $ZrCH_3^+(^3E) \rightarrow ZrCH^+(^3\Phi) + H_2(^1\Sigma_g^+)$ is spin-allowed, but the ground state of these products are $ZrCH^+(^1\Sigma^+) + H_2(^1\Sigma_g^+)$. Overall, a complete exposition of the PES for the $Zr^+(^4F) + CH_4$ reaction requires consideration of both quartet and doublet surfaces. Results for such calculations are listed in Table 4 and are detailed in the following.

Some of the details for the PES for the dehydrogenation of methane by Zr^+ have been previously investigated theoretically by Blomberg et al.[33] They investigated the C−H bond insertion step using geometry optimizations at an SCF level followed by MCPF energy calculations. The Hay−Wadt relativistic ECP was used on the metals along with double-ζ basis on C and H. They also applied an empirical correction for zero point, basis set, and correlation effects to their final values.

The potential energy surfaces for the reaction of $Zr^+(^4F)$ and $Zr^+(^2D)$ with methane are shown in Figure 5. The initial interaction of Zr^+ with CH_4 is attractive because of the long-

TABLE 4: B3LYP/HW/6-311++G(3df,3p) Calculated Energies of Intermediates and Transition States

species	state	E (hartree)	ZPE (hartree)	E + 0.9804ZPE	E_{rel} (eV)
$Zr^+(^4F_{3/2}) + CH_4$					0.0
$Zr^+(^4F) + CH_4$		−86.719 035	0.044 503	−86.675 404	0.094
$Zr^+(^2D) + CH_4$		−86.703 975	0.044 503	−86.660 344	0.504
$Zr^+(CH_4)$, **1**	$^4A_1$	−86.747 691	0.044 991	−86.703 582	−0.673
	^2E	−86.734 756	0.044 816	−86.690 818	−0.325
$HZrCH_3^+$, **2**	^2A	−86.754 444	0.037 422	−86.717 755	−1.058
	$^4A'$	−86.680 883	0.036 591	−86.645 009	0.921
$(H)_2ZrCH_2^+$, **3**	$^2A'$	−86.699 598	0.032 368	−86.667 864	0.299
	$^2A''$	−86.635 669	0.036 084i		*a*
	^4A	−86.611 270	0.028 411	−86.583 416	2.597
	^4B	−86.598 672	0.029 236	−86.570 009	2.962
$(H_2)ZrCH_2^+$, **4**	^2A	−86.720 806	0.037 130	−86.684 404	−0.151
	^4A	−86.682 340	0.034 643	−86.648 376	0.829
$ZrCH_2^+ + H_2$	^2A	−86.698 184	0.031 059	−86.667 734	0.303
	^4A	−86.668 244	0.030 818	−86.638 030	1.111
TS **1/2**	$^2A'$	−86.715 470	0.037 492	−86.678 713	0.004
	$^4A''$	−86.675 789	0.036 872	−86.639 639	1.067
TS **2/4**	^2A	−86.716 192	0.035 344	−86.681 541	−0.073
	^4A	−86.660 078	0.034 013	−86.626 732	1.418
TS **2/3**	^2A	−86.698 360	0.031 834	−86.667 150	0.319
	^4A	−86.607 243	0.028 152	−86.579 643	2.700
TS **3/4**	^4A	−86.603 013	0.028 000	−86.575 562	2.811

[a] Imaginary frequency, collapses to $HZrCH_3^+$.

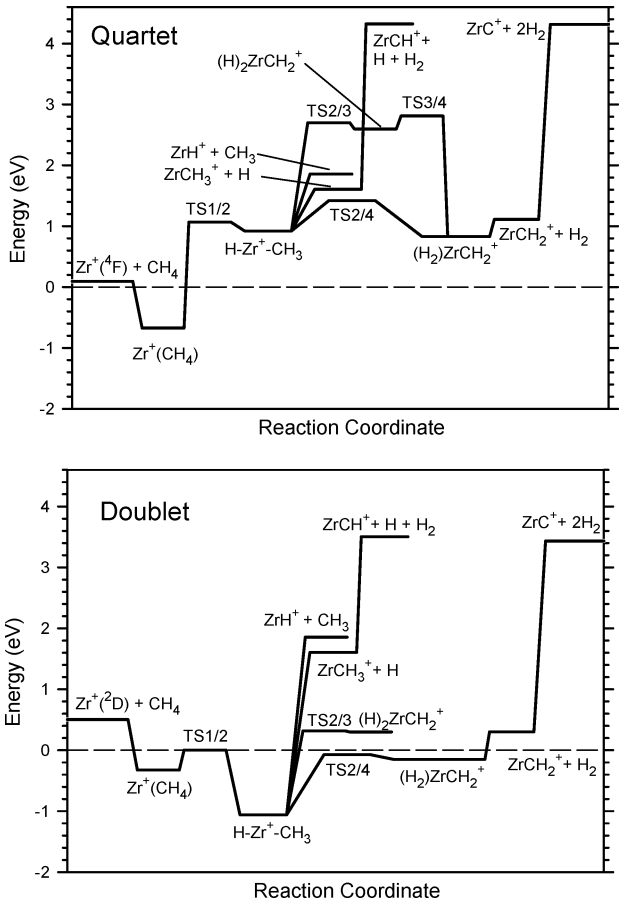

Figure 5. $[ZrCH_4]^+$ potential energy surfaces for quartet (a, top) and doublet (b, bottom) spin derived from theoretical results described in the text and listed in Table 4. The dashed lines show the energy of the ground-state $Zr^+(^4F_{3/2})$ + CH_4 reactants.

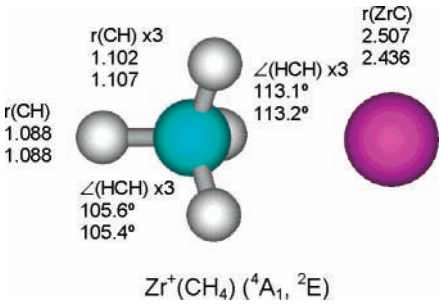

Figure 6. Ground-state geometries of intermediate **1**, $Zr(CH_4)^+$, for both the quartet ground state ($^4A_1$, upper values) and the lowest energy doublet state (^2E, lower values). Bond lengths are in angstroms and angles are in degrees. All structures were optimized at the B3LYP/HW/6-311++G(3df,3p) level of theory.

range ion-induced dipole interaction. Thus, there is a potential well corresponding to the $Zr^+(CH_4)$ adduct, structure **1**, on both the quartet and doublet surface. We find a $^4A_1$ ground state having C_{3v} symmetry geometry shown in Figure 6. Blomberg et al. assumed that the $Zr^+(CH_4)$ complex had C_{2v} symmetry and found a $^4B_1$ ground state. In our calculations, this species is a transition state lying 0.71 eV higher in energy and having one imaginary frequency that connects it with the η^3 ground-state complexes. We find that the depth of the $Zr^+(^4F)-CH_4$ potential well is 0.67 eV relative to the reactants, Table 4. This is comparable to the interaction calculated by Blomberg et al. of 0.71 eV (0.45 eV before the empirical correction). There is also a $Zr^+(CH_4)$ complex having doublet spin. The ^2E ground state has C_{3v} symmetry and lies in a well 0.33 eV below ground-state reactants and 0.73 eV below the calculated $Zr^+(^2D)$ + CH_4 asymptote, such that the bond energies on the quartet and doublet surfaces are nearly equivalent. Again the η^2 complex having C_{2v} symmetry is a transition state, with a $^2B_2$ state having the lowest energy and lying only 0.10 eV above the η^3 ^2E complex. $^2B_1$ and $^2A_1$ states, both transition states, were also found and lie 0.23 and 0.46 eV above the η^3 ^2E complex.

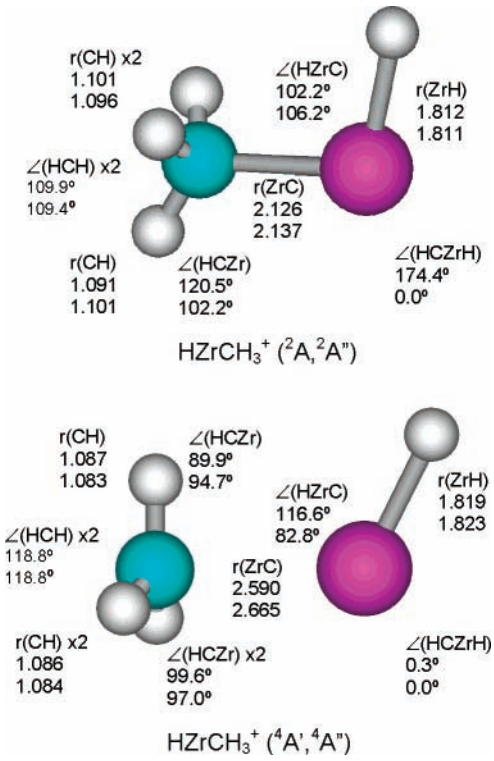

Figure 7. Ground-state geometries of intermediate **2**, $HZrCH_3^+$, for two doublet states (^2A, upper values; $^2A''$, lower values; note that the methyl group is actually rotated 60° from the structure shown) and the lowest energy quartet states ($^4A'$, upper values; $^4A''$, lower values). Bond lengths are in angstroms and angles are in degrees. All structures were optimized at the B3LYP/HW/6-311++G(3df,3p) level of theory.

As the reactants approach more closely, the system passes through a transition state (TS **1/2**) as Zr^+ inserts into one C−H bond of CH_4 to form the H−Zr^+−CH_3 intermediate, structure **2**. The ground state of this intermediate is ^2A and has the geometry shown in Figure 7. The bond distances are comparable to those calculated by Blomberg et al.[33] for a $^2A'$ state, r(ZrH) = 1.84 Å, r(ZrC) = 2.18 Å, and ∠(HZrC) = 108.7°. One HZrCH dihedral angle is 174.4°, such that the complex does not quite have C_s symmetry. Imposition of C_s symmetry (∠HZrCH = 180.0°) yields a $^2A''$ state lying 0.11 eV higher in energy and having one imaginary frequency. We also found another $^2A''$ species lying 0.08 eV above the ^2A ground state but where the HZrCH dihedral angle is 0.0°. Details of this geometry are also provided in Figure 7. Searches for a $^2A'$ state yielded much higher energy species. The $HZrCH_3^+$ species represents the global minimum on the entire PES, Figure 5, and lies in a well 1.06 eV deep compared to ground-state reactants. After corrections for ZPE, basis set, and correlation effects, Blomberg et al. calculate that this species is stable by 1.22 eV (0.53 before the corrections). Lying high above this complex is the analogous species on the quartet surface. The lowest energy quartet complex is a $^4A'$ lying 1.98 eV above the ^2A ground state (0.92 eV above the ground-state reactants). In addition, there is a low-lying $^4A''$ species lying another 0.09 eV higher in energy. This latter species was found to have one imaginary frequency corresponding to rotation of the methyl group about

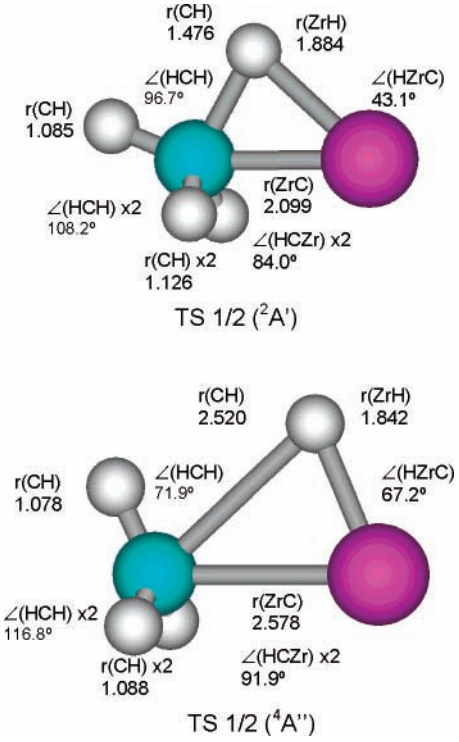

Figure 8. Ground-state geometries of transition state **1/2** on the doublet ($^2A'$, upper panel) and quartet ($^4A''$, lower panel) surfaces. Bond lengths in Å and angles in degrees. All structures were optimized at the B3LYP/HW/6-311++G(3df,3p) level of theory.

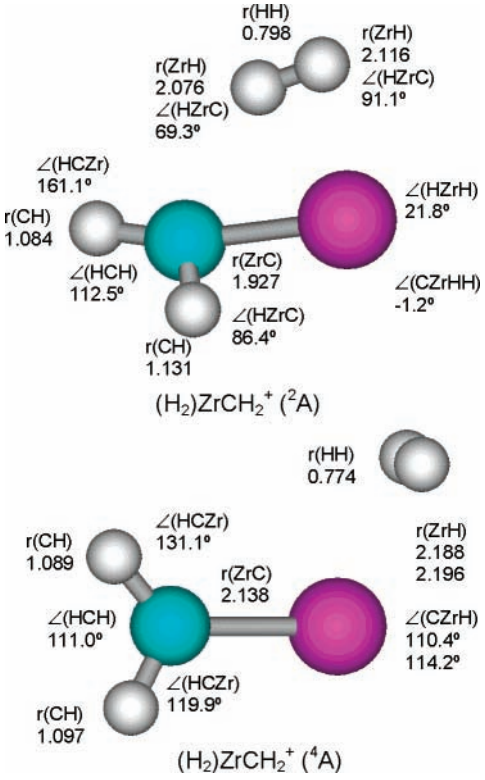

Figure 9. Ground-state geometries of intermediate **4**, $(H_2)ZrCH_2^+$, for the doublet ground state (^2A, upper panel) and the lowest energy quartet state (^4A, lower panel). Bond lengths are in angstroms and angles are in degrees. All structures were optimized at the B3LYP/HW/6-311++G(3df,3p) level of theory.

the Zr−C bond axis. As shown in Figure 7, the quartet species are distinguished from the doublets in that the ZrC bond lengths are quite long, such that the methyl group is nearly planar, as it would be for a free methyl group. Indeed, the calculated bond energy, $D_0(HZr^+-CH_3, {}^4A')$, is only 0.94 eV, compared with that for the ^2A ground state, 2.91 eV.

As noted above, the system passes through TS **1/2** in order to reach the inserted intermediate **2** from the simple adduct **1**. On the doublet surface, ^{2}TS **1/2**, shown in Figure 8, has C_s symmetry and the expected appearance of an incipient insertion. It is calculated to lie 0.004 eV above ground-state reactants, 0.33 eV above $Zr^+(CH_4)(^2E)$, and 1.06 eV above $HZrCH_3^+$-(^2A). After corrections for ZPE, basis set, and correlation effects, the calculations of Blomberg et al.[33] find this TS to lie at a comparable energy, 0.01 eV above reactants, and 1.23 eV above $HZrCH_3^+(^2A)$. On the quartet surface, ^{4}TS **1/2** lies quite high in energy, 0.15 eV above the $HZrCH_3^+(^4A')$ intermediate. The structure is shown in Figure 8.

The $HZrCH_3^+$ intermediate can evolve into the $(H_2)ZrCH_2^+$ intermediate **4**, which then loses H_2 to form $ZrCH_2^+$, in one of two conceivable pathways: (1) an α-H shift to form the dihydride, $(H)_2ZrCH_2^+$ (**3**), or (2) a four-centered transition state forming an incipient H_2 bond directly. The latter is found to be the lowest energy pathway. On the doublet surface, the $(H_2)ZrCH_2^+$ intermediate **4** lies 0.15 eV below ground-state reactants and 0.45 eV below the calculated asymptote for $ZrCH_2^+(^2A') + H_2$ products. On the quartet surface, **4** lies 0.83 eV above ground-state reactants and 0.28 eV below the calculated asymptote for $ZrCH_2^+(^4B_2) + H_2$ products. The structures of these two intermediates are distinct as shown in Figure 9. The quartet species is close to having C_s symmetry, whereas the doublet species has no symmetry. In both cases, the H−H bond distances are close to those of free dihydrogen, calculated to be 0.742 Å at this level of theory. Clearly, loss of dihydrogen from either the doublet or quartet state of **4** can occur with no barrier.

The transition state for evolving from intermediate **2** to **4**, TS **2/4**, is shown in Figure 10. It can be viewed as a four-centered transition state, although clearly the hydrogen atom being transferred is maintaining good contact with the zirconium atom. This is consistent with multicenter transition states elucidated for reactions of hydrocarbons with first-row transition metal ions.[34,54−57] On the doublet surface, ^{2}TS **2/4** lies 0.07 eV below the energy of the ground state reactants and only 0.08 eV above **4**(^2A). On the quartet surface, ^{4}TS **2/4** lies 1.42 eV above the energy of the ground-state reactants and 0.59 eV above **4**(^4A). The quartet transition state is close to having C_s symmetry, but there is a distinct distortion reducing the symmetry, Figure 10.

Alternatively, dehydrogenation can involve formation of a dihydride intermediate that is formed via TS **2/3**, a three-centered transition state involving migration of a H-atom from C to Zr. On the doublet surface, ^{2}TS **2/3** lies 0.32 eV above ground-state reactants, and only 0.02 eV above the $(H)_2ZrCH_2^+$ **3** intermediate, which has a $^2A'$ ground state. A $^2A''$ state for this intermediate, lying 1.84 eV higher in energy, was also located but found to have an imaginary frequency that leads to collapse to the ^2A state of $HZrCH_3^+$. The geometries of $(H)_2ZrCH_2^+$ **3** ($^2A'$) and ^{2}TS **2/3** are shown in Figure 11. On the quartet surface, these species lie much higher in energy. $(H)_2ZrCH_2^+$ **3** now has C_2 symmetry and both a ^4A and a ^4B state, lying 2.60 and 2.96 eV above ground-state reactants, respectively. ^{4}TS **2/3** lies 0.10 eV above the ^4A state, Figure 5. The geometries of these species are shown in Figure 12. The transition state leading from **3** to the dihydrogen complex, **4**, TS **3/4**, was located on the quartet surface and lies 0.21 eV above **3**. On the doublet surface, no suitable transition state was located. Small distortions away from C_s symmetry collapsed to

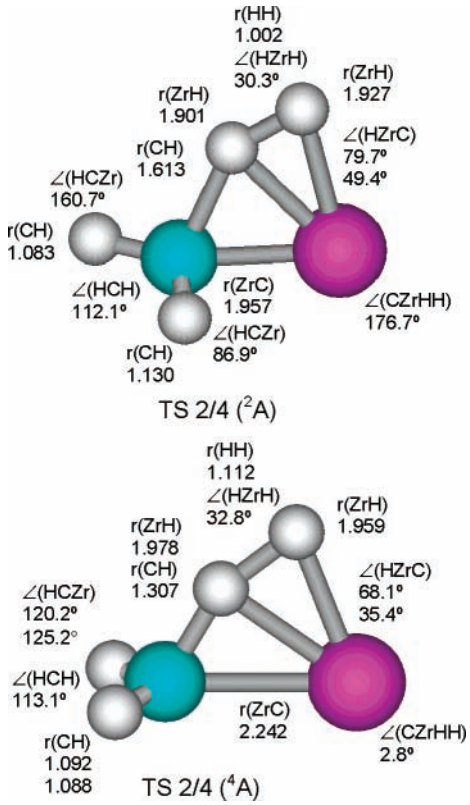

Figure 10. Ground-state geometries of transition state **2/4** on the doublet surface (^{2}A, upper panel) and quartet surface (^{4}A, lower panel). Bond lengths are in angstroms and angles are in degrees. All structures were optimized at the B3LYP/HW/ 6-311++G(3df,3p) level of theory.

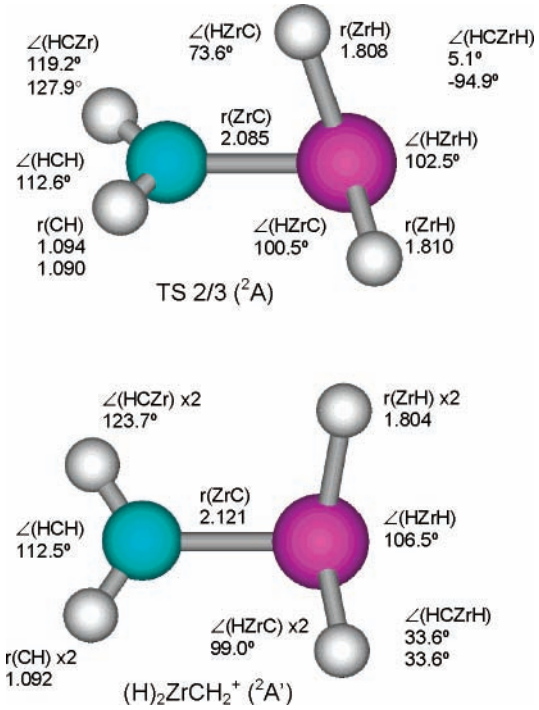

Figure 11. Ground-state geometries of transition state **2/3** on the doublet surface (^{2}A, upper panel) and intermediate **3**, $(H)_2ZrCH_2^+$ (^{2}A′, lower panel). Bond lengths are in angstroms and angles are in degrees. All structures were optimized at the B3LYP/HW/ 6-311++G(3df,3p) level of theory.

either **2** or **4**. As this pathway is not the lowest energy path for dehydrogenation, characterization of ^{2}TS **3/4** was not pursued further.

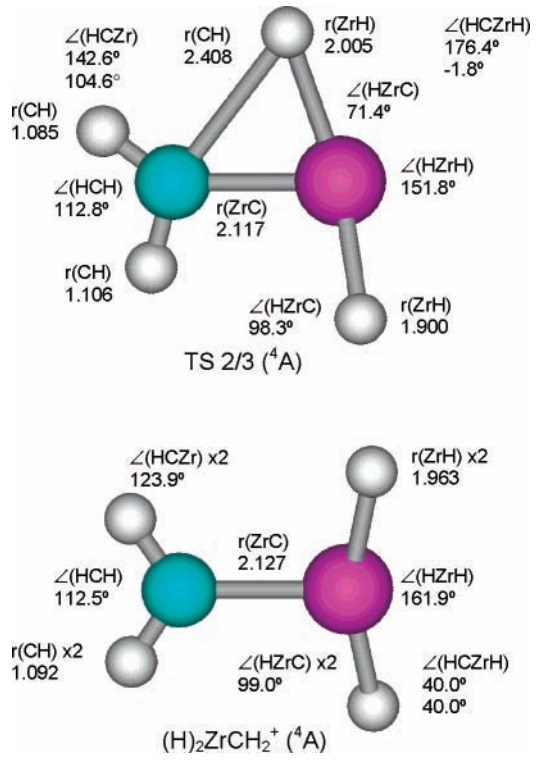

Figure 12. Ground-state geometries of transition state **2/3** on the quartet surface (^{4}A, upper panel) and intermediate **3**, $(H)_2ZrCH_2^+$ (^{4}A, lower panel). Bond lengths are in angstroms and angles are in degrees. All structures were optimized at the B3LYP/HW/ 6-311++G(3df,3p) level of theory.

6. Discussion

6.1. Reaction Mechanism. The potential energy surfaces characterized here are consistent with previous explanations for the activation of alkanes by transition metal cations.[1,5,20] The process starts by an oxidative addition mechanism in which Zr^+ inserts into a C−H bond to form the $H-Zr^+-CH_3$ intermediate **2**. The ground state of this intermediate has doublet spin, and the analogous quartet intermediate is too high in energy to allow the dehydrogenation reaction 5 at the low energies observed experimentally, Figures 1 and 2. Thus, at low energies, there must be a change in spin from quartet to doublet as the reactants interact strongly with the hydrocarbon to form the $H-Zr^+-CH_3$ intermediates, Figure 5. On the basis of the present results, it appears that this spin conversion is not particularly efficient in the zirconium systems as the cross section for $ZrCH_2^+$ formation is about 30−50 times smaller than the collision rate at energies just above the maximum cross section.

Once the $H-Zr^+-CH_3$ intermediate in its ground doublet state is formed, all subsequent rearrangements and the formation of all products can then evolve along doublet surfaces. This is illustrated by the strong competition observed between the formation of the thermodynamically favored products, $ZrCH_2^+ + H_2$, and the $ZrH^+ + CH_3$ product in the methane reaction system. This indicates that the latter channel is kinetically favored and that these reactions pass through a common intermediate. The $H-Zr^+-CH_3(^2A)$ intermediate is an obvious choice as ZrH^+ formation can occur by simple bond cleavage at elevated kinetic energies, whereas H_2 elimination must occur by a more restricted transition state.

The H_2 elimination process occurs by a multicenter transition state, TS **2/4**, to yield $(H_2)ZrCH_2^+(^2A)$, intermediate **4**, which then easily loses the dihydrogen ligand. An alternate pathway

on both the doublet and quartet surfaces is rearrangement of the intermediate through an α-H transfer to form the dihydride intermediate **3**, $(H)_2M^+(CH_2)$ species, which then reductively eliminates H_2. The present calculations characterize both pathways and find that the former is the lowest energy path on both the doublet and quartet surfaces, but only the doublet surface pathway can account for the observed reactivity at low energy. Indeed, examination of the doublet potential energy surface shows that neither ^{2}TS **1/2** nor ^{2}TS **2/4** has energies above the calculated $ZrCH_2^+(^2A) + H_2(^1\Sigma_g^+)$ product asymptote. Therefore, the thresholds observed for this product ion can be attributed to the overall endothermicity of the process rather than to a barrier along the PES. This is consistent with the observation that the threshold shifts according to the expected zero point energy differences in the CH_4 and CD_4 systems.

At higher energies, the $H-Zr^+-CH_3$ intermediate decomposes by cleavage of the Zr−H and Zr−C bonds to form the primary $ZrCH_3^+$ and ZrH^+ products. Although these channels have similar energetics, the latter product is favored as it can conserve angular momentum more easily.[58] At higher energies, ZrC^+ and $ZrCH^+$ are formed by subsequent dehydrogenation and H atom loss processes from the primary $ZrCH_2^+$ and $ZrCH_3^+$ products. The thermochemistry determined above shows that dehydrogenation of these species requires 3.25 ± 0.13 and 0.95 ± 0.27 eV, respectively. The large difference is because the formal bond order changes little in going from $Zr^+{=}CH_2$ to $Zr^+{=}C$, but changes from 1 to 3 in the transition from Zr^+-CH_3 to $Zr^+{\equiv}CH$, Figure 4. It is interesting to note that H atom loss from $ZrCH_3^+$, which leads to the second feature in the $ZrCH_2^+$ cross sections, Figure 1, requires 2.41 ± 0.17 eV. This process is still observed even though dehydrogenation is a much lower energy channel. This indicates that H-atom loss is kinetically more favorable than H_2 elimination, as expected.

The potential energy surfaces calculated here show that the elimination of H_2 from $H-Zr^+-CH_3$ occurs by passing over a four-center transition state, calculated to lie about 0.43 eV below the energy of the products. Another way of understanding this step is to consider the reverse reaction, i.e., H_2 activation by $ZrCH_2^+$. The following discussion is consistent with simple molecular orbital ideas developed for the activation of H_2 and CH_4 by metal oxide ions.[59] As discussed in detail elsewhere,[1,2] activation of covalent bonds at transition metal centers is most facile when the metal has an empty s-like valence orbital to accept the pair of electrons in the covalent bond, and when it has a pair of valence dπ-like electrons to donate into the antibonding orbital of the bond to be broken. For the metal methylidene cations, Bauschlicher et al.[30] have characterized the valence molecular orbitals (MOs) as $1a_1$ and $1b_1$ M−C bonding; $1a_2$, $1b_2$, and $2a_1$ d-like nonbonding; a $3a_1$ s-like nonbonding; and $2b_1$ and $4a_1$ antibonding orbitals. For these species, the most likely acceptor orbital is the $3a_1$ MO and the π-donor orbital is one of the nonbonding MOs. In the calculations of Bauschlicher et al.,[30] the ground state of $ZrCH_2^+$ is $^2A_1$ with a $(1a_1)^2(1b_1)^2(1a_2)^0(1b_2)^0(2a_1)^1(3a_1)^0$ electron configuration and there is a low-lying $^2A_2$ state with a configuration of $(1a_1)^2(1b_1)^2(1a_2)^1(1b_2)^0(2a_1)^0(3a_1)^0$.[30] The present calculations indicate that $ZrCH_2^+$ distorts, Figure 3, such that the a_1 and b_2 orbitals collapse to a′ symmetry, and the b_1 and a_2 orbitals become a″ symmetry, which leads to the $^2A'$ and $^2A''$ states, respectively. Nevertheless, the overall character of the orbitals is maintained and neither of these states occupies the $3a_1$ acceptor orbital. Thus, the interaction of H_2 with $ZrCH_2^+$ in a doublet state is attractive and allows facile activation of H_2 across the Zr−C bond to form $H-Zr^+-CH_3$. This is indicated by the low barrier for oxidative addition of H_2 to $ZrCH_2^+$, Figure 5, only 0.08 eV.

As noted above, the magnitude of the cross section for ZrH^+ exceeds the depletion in the $ZrCH_2^+$ cross section, suggesting that there is another pathway available to form $ZrH^+ + CH_3$ (reaction 2) at higher energies. This could be a direct abstraction reaction or a process that remains on the quartet surface. As shown in Figure 5a, species remaining on the quartet surface are likely to re-form reactants, but activation of the C−H bond would lead primarily to reaction 2 as this process is entropically favored and energetically requires only a little more energy than passing through ^{4}TS **2/4**.

6.2. Reactivity Differences between Zr^+ and Ti^+. The kinetic energy dependences of the reactions of Ti^+ (the first-row transition metal congener of Zr^+) with CH_4 have been studied previously.[35] The differences in the reactivity of Ti^+ and Zr^+ can be summarized fairly succinctly. First, the efficiency of the dehydrogenation processes differs dramatically between the two metals. Reaction 5 is endothermic, but still has an appreciable cross section, whereas the analogous reaction for $Ti^+(^4F)$ is much less efficient, with an apparent threshold near 1 eV and a maximum cross section of about 1×10^{-18} cm^2 near 2 eV. (However, $Ti^+(^2F)$ lying 0.593 eV higher in energy exhibits reactivity much like $Zr^+(^4F)$ with a threshold for dehydrogenation of 0.14 eV and a maximum cross section of about 2.5×10^{-16} cm^2 near 1.5 eV.) Second, subsequent dehydrogenation of primary products (forming species such as ZrC^+ and $ZrCH^+$) is pronounced in the zirconium systems. Analogous processes are observed in the titanium systems but are much less efficient.

Most of these differences in reactivity can be understood simply on the basis of differences in thermochemistry. The hydride and methyl BDEs of titanium and zirconium cations are similar: compare $D_0(Ti^+-H) = 2.31 \pm 0.11$ eV and $D_0(Ti^+-CH_3) = 2.22 \pm 0.03$ eV[9] with the values in Table 1. In contrast, the ZrC^+, $ZrCH^+$, and $ZrCH_2^+$ bonds are stronger than the titanium analogues by 0.8 ± 0.2 eV.[9] These bond energies are also compared in Figure 4. Thus, formation of all products but MH^+ and MCH_3^+ are energetically more favorable in the zirconium system by over 0.8 eV. This clearly explains the second difference noted above, the relative efficiency of the subsequent dehydrogenation processes. To a large extent, these energy differences also explain the first point, the differences in the primary dehydrogenation channels. Dehydrogenation of methane by Ti^+ is energetically more costly than when induced by Zr^+. Reaction of $Ti^+(^2F)$ gains back about 0.6 eV of this energy, making it energetically similar to $Zr^+(^4F)$; however, this excited state is over 200 times more reactive than ground-state $Ti^+(^4F)$. This suggests that even though the coupling between the doublet and quartet surfaces of Zr^+ is not complete, this coupling is much better than for the first-row congener.

7. Conclusion

Ground-state Zr^+ ions are found to be moderately reactive with CH_4, yielding dehydrogenation at low energies in a slightly endothermic process. At high energies, the dominant process is C−H bond cleavage to form $ZrH^+ + CH_3$, although there are also contributions from $ZrCH_3^+$ and products that result from dehydrogenation of the primary products, $ZrCH^+$ and ZrC^+. The endothermic reaction cross sections are modeled to yield 0 K bond dissociation energies for several Zr−ligand cations, as summarized in Table 1. Reasonable agreement is found for these values compared with previous experimental and theoretical work and B3LYP/HW/6-311++G(3df,3p) calculations conducted here.

The mechanism for the reactions of Zr^+ with methane is discussed in detail and elucidated by fairly complete calculations of the intermediates and transition states along both doublet and quartet potential energy surfaces. These considerations show that the mechanism involves initial C−H bond activation by Zr^+, which involves crossing from the quartet reactant surface to a doublet spin surface. This forms a $H-Zr^+-CH_3$ intermediate that undergoes dehydrogenation through a four-centered transition state at low collision energies and by simple bond cleavage at high energies. When compared to Ti^+, the first-row transition metal congener, Zr^+ is found to be much more reactive. This can be attributed to much stronger π-bonds for the second-row metal ion and probably to more efficient coupling between surfaces of different spin.

Acknowledgment. This research is supported by the National Science Foundation, Grant CHE-0135517. We thank Sae-Young Shin and D. L. Steele for helping to acquire some of the data.

References and Notes

(1) Armentrout, P. B. In *Selective Hydrocarbon Activation: Principles and Progress*; Davies, J. A., Watson, P. L., Greenberg, A., Liebman, J. F., Eds.; VCH: New York, 1990; p 467. Armentrout, P. B. In *Gas-Phase Inorganic Chemistry*; Russell, D. H., Ed.; Plenum: New York, 1989; p 1. Armentrout, P. B.; Beauchamp, J. L. *Acc. Chem. Res.* **1989**, *22*, 315.

(2) Armentrout, P. B. *Science* **1991**, *251*, 175. Armentrout, P. B. *Annu. Rev. Phys. Chem.* **1990**, *41*, 313.

(3) Weisshaar, J. C. *Adv. Chem. Phys.* **1992**, *82*, 213. Weisshaar, J. C. *Acc. Chem. Res.* **1993**, *26*, 213.

(4) van Koppen, P. A. M.; Kemper, P. R.; Bowers, M. T. *J. Am. Chem. Soc.* **1992**, *114*, 1083, 10941. van Koppen, P. A. M.; Kemper, P. R.; Bowers, M. T. In *Organometallic Ion Chemistry*; Freiser, B. S., Ed.; Kluwer: Dordrecht, 1995; pp 157−196.

(5) Allison, J. *Prog. Inorg. Chem.* **1986**, *34*, 627. Squires, R. R. *Chem. Rev.* **1987**, *87*, 623. *Gas-Phase Inorganic Chemistry*; Russell, D. H., Ed.; Plenum: New York, 1989. Eller, K.; Schwarz, H. *Chem. Rev.* **1991**, *91*, 1121.

(6) Armentrout, P. B.; Georgiadis, R. *Polyhedron* **1988**, *7*, 1573.

(7) Armentrout, P. B. *ACS Symp. Ser.* **1990**, *428*, 18.

(8) Armentrout, P. B.; Clemmer, D. E. In *Energetics of Organometallic Species*; Simoes, J. A. M., Beauchamp, J. L., Eds.; Kluwer: Dordrecht, 1992; p 321.

(9) Armentrout, P. B.; Kickel, B. L. In *Organometallic Ion Chemistry*; Freiser, B. S., Ed.; Kluwer: Dordrecht, 1995; pp 1−45.

(10) *Organometallic Ion Chemistry*; Freiser, B. S., Ed.; Kluwer: Dordrecht, 1995.

(11) Crabtree, R. H. *Chem. Rev.* **1985**, *85*, 245.

(12) Sunderlin, L. S.; Armentrout, P. B. *J. Am. Chem. Soc.* **1989**, *111*, 3845.

(13) Kickel, B. L.; Armentrout, P. B. *J. Am. Chem. Soc.* **1995**, *117*, 4057.

(14) Sievers, M. R.; Chen, Y.-M.; Haynes, C. L.; Armentrout, P. B. *Int. J. Mass Spectrom.* **2000**, *195/196*, 149.

(15) Armentrout, P. B.; Chen, Y.-M. *J. Am. Soc. Mass Spectrom.* **1999**, *10*, 821.

(16) Chen, Y.-M.; Armentrout, P. B. *J. Phys. Chem.* **1995**, *99*, 10775.

(17) Chen, Y.-M.; Armentrout, P. B. *J. Am. Chem. Soc.* **1995**, *117*, 9291.

(18) Chen, Y.-M.; Sievers, M. R.; Armentrout, P. B. *Int. J. Mass Spectrom. Ion Processes* **1997**, *167/168*, 195.

(19) Chen, Y.-M.; Armentrout, P. B. *J. Phys. Chem.* **1995**, *99*, 11424.

(20) Armentrout, P. B. *Organometallic Bonding and Reactivity*; Brown, J. M., Hofmann, P., Eds.; *Topics in Organometallic Chemistry*; Springer-Verlag: Berlin, 1999; Vol. 4, pp 1−45.

(21) Ranasinghe, Y. A.; MacMahon, T. J.; Freiser, B. S. *J. Phys. Chem.* **1991**, *95*, 7721.

(22) Sievers, M. R.; Chen, Y.-M.; Elkind, J. L.; Armentrout, P. B. *J. Phys. Chem.* **1996**, *100*, 54.

(23) Sievers, M. R.; Chen, Y.-M.; Armentrout, P. B. *J. Chem. Phys.* **1996**, *105*, 6322.

(24) Bushnell, J. E.; Kemper, P. R.; van Koppen, P.; Bowers, M. T. *J. Phys. Chem.* **2001**, *105*, 2216.

(25) Ranatunga, D. R. A.; Freiser, B. S. *Chem. Phys. Lett.* **1995**, *233*, 319.

(26) Schilling, J. B.; Goddard, W. A., III; Beauchamp, J. L. *J. Am. Chem. Soc.* **1987**, *109*, 5565.

(27) Pettersson, L. G. M.; Bauschlicher, C. W., Jr.; Langhoff, S. R.; Partridge, H. *J. Chem. Phys.* **1987**, *87*, 481.

(28) Das, K. K.; Balasubramanian, K. *J. Mol. Spectrosc.* **1991**, *148*, 250.

(29) Siegbahn, P. E. M.; Blomberg, M. R. A.; Svensson, M. *Chem. Phys. Lett.* **1994**, *223*, 35.

(30) Bauschlicher, C. W., Jr.; Partridge, H.; Sheehy, J. A.; Langhoff, S. R.; Rosi, M. *J. Phys. Chem.* **1992**, *96*, 6969.

(31) Blomberg, M. R. A.; Siegbahn, P. E. M. *ACS Symp. Ser.* **1998**, *677*, 197.

(32) Bauschlicher, C. W., Jr.; Langhoff, S. R.; Partridge, H.; Barnes, L. A. *J. Chem. Phys.* **1989**, *91*, 2399.

(33) Blomberg, M. R. A.; Siegbahn, P. E. M.; Svensson, M. *J. Phys. Chem.* **1994**, *98*, 2062.

(34) Perry, J. K. Ph.D. Thesis, Caltech, 1994.

(35) Sunderlin, L. S.; Armentrout, P. B. *J. Phys. Chem.* **1988**, *92*, 1209.

(36) Ervin, K. M.; Armentrout, P. B. *J. Chem. Phys.* **1985**, *83*, 166.

(37) Schultz, R. H.; Armentrout, P. B. *Int. J. Mass Spectrom. Ion. Processes* **1991**, *107*, 29.

(38) Gerlich, D. *Adv. Chem. Phys.* **1992**, *82*, 1.

(39) Chesnavich, W. J.; Bowers, M. T. *J. Phys. Chem.* **1979**, *83*, 900.

(40) Armentrout, P. B. *Advances in Gas-Phase Ion Chemistry*; Adams, N. G., Babcock L. M., Eds.; JAI: Greenwich, 1992; Vol. 1, pp. 83−119.

(41) Shimanouchi, T. *Table of Molecular Vibrational Frequencies, Consolidated*; National Bureau of Standards: Washington, DC, 1972; Vol. I.

(42) Becke, A. D. *J. Chem. Phys.* **1993**, *98*, 5648.

(43) Lee, C.; Yang, W.; Parr, R. G. *Phys. Rev. B* **1988**, *37*, 785.

(44) Stephens, P. J.; Devlin, F. J.; Chabalowski, C. F.; Frisch, M. J. *J. Phys. Chem.* **1994**, *98*, 11623.

(45) Frisch, M. J.; Trucks, G. W.; Schlegel, H. B.; Scuseria, G. E.; Robb, M. A.; Cheeseman, J. R.; Zakrzewski, V. G.; Montgomery, J. A., Jr.; Stratmann, R. E.; Burant, J. C.; Dapprich, S.; Millam, J. M.; Daniels, A. D.; Kudin, K. N.; Strain, M. C.; Farkas, O.; Tomasi, J.; Barone, V.; Cossi, M.; Cammi, R.; Mennucci, B.; Pomelli, C.; Adamo, C.; Clifford, S.; Ochterski, J.; Petersson, G. A.; Ayala, P. Y.; Cui, Q.; Morokuma, K.; Malick, D. K.; Rabuck, A. D.; Raghavachari, K.; Foresman, J. B.; Cioslowski, J.; Ortiz, J. V.; Baboul, A. G.; Stefanov, B. B.; Liu, G.; Liashenko, A.; Piskorz, P.; Komaromi, I.; Gomperts, R.; Martin, R. L.; Fox, D. J.; Keith, T.; Al-Laham, M. A.; Peng, C. Y.; Nanayakkara, A.; Gonzalez, C.; Challacombe, M.; Gill, P. M. W.; Johnson, B. G.; Chen, W.; Wong, M. W.; Andres, J. L.; Gonzalez, C.; Head-Gordon, M.; Replogle, E. S.; Pople, J. A. *Gaussian 98*; Gaussian, Inc.: Pittsburgh, PA, 1998.

(46) Foresman, J. B.; Frisch, Æ. *Exploring Chemistry with Electronic Structure Methods*, 2nd ed.; Gaussian: Pittsburgh, 1996.

(47) Hay, P. J.; Wadt, W. R. *J. Chem. Phys.* **1985**, *82*, 299.

(48) The basis set for Zr was obtained from the Extensible Computational Chemistry Environment Basis Set Database, Version 10/29/02, as developed and distributed by the Molecular Science Computing Facility, Environmental and Molecular Sciences Laboratory, which is part of the Pacific Northwest Laboratory, P. O. Box 999, Richland, WA 99352, and funded by the U.S. Department of Energy. The Pacific Northwest Laboratory is a multiprogram laboratory operated by Battelle Memorial Institute for the U.S. Department of Energy under Contract No. DE-AC06-76RLO 1830.

(49) Moore, C. E. *Atomic Energy Levels*; NSRDS-NBS; 1971; Vol. III, p 35.

(50) Zhang, X.-G.; Liyanage, R.; Armentrout, P. B. *J. Am. Chem. Soc.* **2001**, *123*, 5563−5575.

(51) Simon, A.; Lemaire, J.; Boissel, P.; Maître, P. *J. Chem. Phys.* **2001**, *115*, 2510−2518.

(52) Holthausen, M. C.; Heinemann, C.; Cornehl, H. H.; Koch, W.; Schwarz, H. *J. Chem. Phys.* **1995**, *102*, 4931−4941.

(53) Aristov, N.; Armentrout, P. B. *J. Am. Chem. Soc.* **1984**, *106*, 4065.

(54) Holthausen, M. C.; Fiedler, A.; Schwarz, H.; Koch, W. *J. Phys. Chem.* **1996**, *100*, 6236.

(55) Holthausen, M. C.; Koch, W. *Helv. Chim. Acta* **1996**, *79*, 1939.

(56) Holthausen, M. C.; Koch, W. *J. Am. Chem. Soc.* **1996**, *118*, 9932.

(57) Yi, S. S.; Blomberg, M. R. A.; Siegbahn, P. E. M.; Weisshaar, J. C. *J. Phys. Chem.* **1998**, *102*, 395.

(58) Aristov, N.; Armentrout, P. B. *J. Phys. Chem.* **1987**, *91*, 6178.

(59) Clemmer, D. E.; Aristov, N.; Armentrout, P. B. *J. Phys. Chem.* **1993**, *97*, 544.